Microstructural Model for Hot Strip Rolling of High-Strength Low-Alloy Steels

M. MILITZER, E.B. HAWBOLT, and T.R. MEADOWCROFT

The microstructural evolution during hot-strip rolling has been investigated in four commercial high-strength low-alloy (HSLA) steels and compared to that of a plain, low-carbon steel. The recrystallization rates decrease as the Nb microalloying content increases, leading to an increased potential to accumulate retained strain during the final rolling passes. The final microstructure and properties of the hot band primarily depend on the austenite decomposition and precipitation during run-out table cooling and coiling. A combined transformation–ferrite-grain-size model, which was developed for plain, low-carbon steels, can be applied to HSLA steels with some minor modifications. The effect of rolling under no-recrystallization conditions (controlled rolling) on the transformation kinetics and ferrite grain refinement has been evaluated for the Nb-containing steels. Precipitation of carbides, nitrides, and/or carbonitrides takes place primarily during coiling, and particle coarsening controls the associated strengthening effect. The microstructural model has been verified by comparison to structures produced in industrial coil samples.

I. INTRODUCTION

WE dedicate this article to the late Professor J. Keith Brimacombe, who passed away suddenly on December 16, 1997. His leadership and vision were instrumental in mounting the hot strip–process modeling research in the Centre for Metallurgical Process Engineering at the University of British Columbia. This research was conducted in collaboration with the American Iron and Steel Institute, the United States Department of Energy, and the National Institute of Standards and Technology. The present article summarizes the results of a physical metallurgy investigation on several high-strength low-alloy (HSLA) steels.

The HSLA steels were developed in the 1960s by microalloying low-carbon steels with Nb, V, and Ti in the 0.01 to 0.1 wt pct range. The increased strength of HSLA steels is attributed to a combination of ferrite grain refinement and precipitation strengthening. The HSLA steels have become a widely used material, in particular for automotive applications and as linepipe grades. Interestingly, while the weight fraction of steel and iron in an average family vehicle has decreased from 74 pct in 1978 to 67 pct in 1997, that of high- and medium-strength steels has increased from 3.7 to 9.1 pct in the same time period.[1] With this increase of approximately 150 pct, higher-strength steels show the biggest gain of any material class in automotive applications, even ahead of aluminum or plastics and plastic composites, which are widely discussed as alternatives to steel for the development of more-fuel-efficient, lightweight vehicles. A significant component of these higher-strength steels are hot-rolled HSLA steels, which are used in high-strength vehicle components such as wheel rims or bumpers.

Microstructural engineering has been increasingly gaining attention, with the goal being to quantitatively link the operational parameters of a hot-strip mill with the properties of the hot band.[2–8] These microstructural process models, which focused initially on plain carbon steels, have only recently been extended to include medium-strength HSLA steels.[8] These model extensions, however, still incorporate a great deal of empiricism, with comparatively tight process ranges of applicability. More fundamentally based process models are required to develop predictive tools to optimize the production of high-quality HSLA steel grades for a wide range of mill designs and processing conditions.

The processing in a hot-strip mill can be subdivided into three principal stages: (1) reheating, (2) rolling (in both the roughing and finishing mill), and (3) cooling (water cooling on the run-out table and coiling). The metallurgical phenomena which occur in these three processing steps are summarized in Table I and can be grouped into three categories: (1) recrystallization and grain growth in austenite, (2) austenite/ferrite phase transformation, and (3) precipitation. Modeling the austenite-to-ferrite transformation on the run-out table and the subsequent precipitation of carbides, nitrides, and/or carbonitrides in ferrite during coiling appear to be of particular importance; both aspects essentially determine the mechanical properties, which depend on the character of the transformation products (ferrite, pearlite, bainite, *etc.*), the ferrite grain size, and the extent of precipitation and solid solution.

Numerous investigations have been conducted to shed light on microstructural evolution in microalloyed steels. These studies have usually separately characterized the effect of microalloying additions on recrystallization,[9–12] precipitation,[13–17] and phase transformation.[18,19] The emphasis of this research was associated primarily with the phenomenon of controlled rolling in Nb-microalloyed steels. Adding Nb to the steel increases the so-called no-recrystallization temperature, the temperature below which recrystallization cannot be completed within the interstand times of a multipass rolling operation. Laboratory investigations reflect quite accurately the roughing mill as well as the plate mill operations, these having relatively low strain rates and interpass times which range from a few seconds to approximately 30 seconds. Extending these laboratory findings to

M. MILITZER, Assistant Professor, E.B. HAWBOLT, Professor Emeritus, and T.R. MEADOWCROFT, Professor, are with the Centre for Metallurgical Process Engineering, The University of British Columbia, Vancouver, BC, Canada V6T 1Z4.

Manuscript submitted July 13, 1999.

Table I. Metallurgical Phenomena during Hot-Strip Rolling of HSLA Steels

Process Step	Metallurgical Phenomena
Reheating	ferrite-to-austenite transformation, grain growth, dissolution of precipitates
Rolling	recrystallization, austenite grain growth, precipitation
Cooling	austenite-to-ferrite transformation, precipitation

the industrial conditions of hot-strip rolling is a challenging task, because of the high strain rates and short interpass times experienced on a tandem finishing mill. An important debate is still underway as to whether the no-recrystallization temperature is associated with the strain-induced precipitation of Nb(CN)[20–23] or with Nb solute drag.[24–27] Moreover, surprisingly little attention has been paid to elucidating the austenite-to-ferrite transformation in HSLA steels for accelerated cooling conditions, in spite of the fact that the technology of accelerated cooling has been widely accepted as the key for ferrite grain refinement and the resulting increase of both the strength and toughness.

This article deals with a comprehensive approach taken to model the microstructural evolution during hot-strip rolling of commercial HSLA steels. All process steps were analyzed, except reheating, where simplified assumptions, such as equilibrium precipitate dissolution, were adopted. With the aid of the experimental observations, a microstructural model for rough and finish rolling, as well as for run-out table cooling and coiling, has been developed. The model is organized according to the three principal metallurgical phenomena, with recrystallization and grain growth being dominant during rough and finish rolling, the austenite-to-ferrite transformation occurring during run-out table cooling, and precipitation taking place during coiling; precipitation in austenite is of minor importance for industrial processing of the steels investigated. This model extends the approach which was proposed earlier for plain, low-carbon steel[28–31] to include selected HSLA steels.

II. EXPERIMENTAL METHODOLOGY

A. *Materials*

The chemical compositions and Ae_3 temperatures[32] of the investigated steels are shown in Table II. The drawing-quality, special-killed (DQSK) steel is an Al-killed plain carbon steel which is included as a reference steel without microalloying additions. The four HSLA steels represent examples of various important microalloying strategies: (1) singly microalloying with V, (2) singly microalloying with Nb, (3) Nb/Ti microalloying with a substoichiometric Ti/N ratio, and (4) Nb/Ti microalloying with an overstoichiometric Ti/N ratio. Further, the two Nb/Ti grades represent different strength classes: Nb/Ti 50 is similar in strength to the singly microalloyed grades, with a minimum yield-strength requirement of approximately 350 MPa (50 ksi), whereas Nb/Ti 80 is a steel having a 550 MPa (80 ksi) minimum yield strength.

B. *Tests*

In order to examine the required microstructural detail, laboratory tests were carried out employing a Gleeble 1500 thermomechanical simulator and a DSI hot-torsion simulator (HTS 100) to reproduce the thermomechanical processing steps of a hot-strip mill. The torsion machine provides the opportunity to simulate the entire process of a hot-strip mill, from reheating to down-coiling.[33] The torsion specimens are 183 mm in length, with a diameter of 14.3 mm; the gage length of the working zone is 12.7 mm, with a diameter of 10 mm. There is feedback temperature control during reheating, employing a spot-welded thermocouple and, during multipass deformation, employing an optical pyrometer. After deformation, the specimens are He gas–cooled to room temperature. As a matter of convenience, microstructural development during coiling has been studied using aging tests, which employ salt baths for short holding times or a conventional furnace for longer holding times. The Gleeble is an excellent tool for quantifying specific microstructure-modifying phenomena; *i.e.*, recrystallization, grain growth, precipitation, and austenite decomposition. Experimental details of the Gleeble work have been published elsewhere.[28–30,34,35] The Gleeble test series of the current research is summarized in Table III, showing the range of parameters evaluated in specific Gleeble tests and the significance of these parameters to microstructural characterization.

In the first series of tests, austenite grain growth was studied using isothermal tests, with the primary goal of establishing suitable reheating conditions for subsequent deformation and transformation tests. Table IV summarizes the reheating conditions and austenite grain sizes employed in this study. The austenite grain sizes are reported as an equivalent volume diameter, which is required for more-fundamental model approaches, as, for example, at least in part, those employed in the transformation model. The volume diameter is obtained by multiplying the measured equivalent area diameter (EQAD) by 1.2, as discussed in detail by Giumelli *et al.*;[36] the mean linear intercept, another frequently employed method to characterize grain sizes, amounts to 80 pct of the EQAD. The design of the austenite reheating tests is complicated by the occurrence of abnormal

Table II. Chemical Composition (Weight Percent) and Ae_3 Temperature (°C)[32] of the Steels

Steel	T_{Ae3}	C	Mn	V	Nb	Ti	Si	Al	N
DQSK	883	0.04	0.30	—	—	—	0.009	0.040	0.0052
V	876	0.045	0.45	0.08	—	0.002	0.069	0.078	0.0072
Nb	860	0.08	0.48	—	0.036	—	0.045	0.024	0.0054
Nb/Ti 50	857	0.07	0.76	—	0.023	0.013	0.014	0.053	0.0067
Nb/Ti 80	843	0.07	1.35	—	0.086	0.047	0.14	0.044	0.0070

Table III. Parameter Range of Gleeble Tests

Test Series	Objective	Parameter Range
Austenite grain growth	establishing reheating conditions	heating rate: 5 °C/s to 100°C/s temperature: 950 °C to 1250 °C holding time: up to 15 min
Single and double hit tests	recrystallization behavior	reheating temperature: 950 °C to 1250°C hit strain: 0.1 to 1.0 strain rate: 0.1 to $10 s^{-1}$ deformation temperature: 900 °C to 1200 °C
Stress relaxation tests	strain-induced precipitation	temperature: 850 °C to 1050 °C
Continuous cooling transformation	austenite decomposition kinetics	reheating temperature: 950 °C to 1150 °C cooling rate: 1°C/s to 250 °C/s retained strain: 0 to 0.6

Table IV. Reheating Conditions Employed and Resulting Austenite Grain Sizes

Steel	Heating Rate, °C/s	Reheating Temperature, °C	Holding Time, s	Volumetric Austenite Grain Size, μm
DQSK	5	950	120	38
	5	1100	120	136
	5	1150	60	190
V	5	950	120	36
	100	1150	0	85
	5	1150	30	120
Nb	5	950	120	18
	100	1100	0	42
	5	1150	30	84
	5	1150	300	260
Nb/Ti 50	5	950	120	18
	5	1150	120	73
Nb/Ti 80	5	950	120	11
	5	1100	60	14
	5	1150	60	29
	5	1200	600	200
	5	1250	600	330

grain growth, which occurs when precipitates begin to dissolve at the so-called grain-coarsening temperature.[29,37]

In the second series of tests, single-hit compression tests were conducted to establish the deformation conditions for static and metadynamic recrystallization. Then, double-hit compression tests were performed to quantify the recrystallization kinetics as a function of the initial austenite grain size, deformation strain, strain rate, and temperature. Recrystallized grain sizes (and subsequent grain growth) were investigated on specimens which were held sufficiently long after a single-hit test to complete recrystallization. Strain-induced precipitation in austenite, as a function of temperature, was evaluated using a stress-relaxation technique.[16,34] Continuous cooling

Table V. Parameters Describing the Boundary Separating Static and Metadynamic Recrystallization

Steel	η (s^{-1})	Z_0 (s^{-1})	υ (μm^{-1})	Q_{def} (kJ/mol)
DQSK	5×10^{15}	0	0.0129	334
V	5×10^{15}	0	0.0129	334
Nb	3.76×10^{19}	0	0.0116	421
Nb/Ti 50	3.76×10^{19}	0	0.0116	421
Nb/Ti 80	8.52×10^{18}	2.3×10^{16}	0.116	442

transformation (CCT) tests, rather than isothermal transformation tests, were conducted for these low-carbon steels to dilatometrically quantify the austenite decomposition kinetics as a function of cooling rate and initial austenite microstructure. The first transformation series examined undeformed samples to quantify the effects of cooling rate and austenite grain size on the transformation kinetics; the second test series also incorporated the role of deformation under no-recrystallization conditions in the austenite. The dilatometer measurements were supplemented with metallographic analysis of the microstructure resulting from the austenite decomposition; in particular, the ferrite grain size was measured as an EQAD. In the final series of tests, aging tests in combination with hardness measurements were made to develop a model for the precipitation-strengthening kinetics in ferrite during coiling. The indirect precipitation studies (aging tests and stress-relaxation tests) were supplemented by selected direct observations of the particle-size distribution, employing transmission electron microscopy (TEM).

III. RECRYSTALLIZATION AND GRAIN GROWTH

A. *Recrystallization Type*

Whether static or metadynamic recrystallization takes place is evaluated based on the flow-stress curves obtained from single-hit tests. The occurrence of a peak in the stress-strain response indicates that dynamic recrystallization takes place. The critical strain (ε_c) for dynamic recrystallization is attained at a strain of five-sixths of the peak strain (ε_p). The potential for dynamic and subsequent interstand (metadynamic) recrystallization can be described with a limiting Zener–Hollomon parameter, which separates those flow curves which exhibit a peak from those without a peak. The Zener–Hollomon parameter is a temperature-compensated strain rate, *i.e.*,

$$Z = \dot{\varepsilon} \exp\left(\frac{Q_{def}}{RT}\right) \qquad [1]$$

where Q_{def} is an effective deformation activation energy. The limiting Zener–Hollomon parameter has the form[28]

$$Z_{lim} = \eta \exp(-\upsilon d_0) + Z_0 \qquad [2]$$

where d_0 is the initial austenite grain size. Table V summarizes the magnitude of the parameters Q_{def}, Z_0, η, and υ used for the steel grades examined in this study. For $Z < Z_{lim}$, interstand metadynamic recrystallization occurs, provided the strain is larger than five-sixths of ε_p, since the effective deformation times are sufficiently long because of low strain rates and/or high temperatures. In general, these conditions

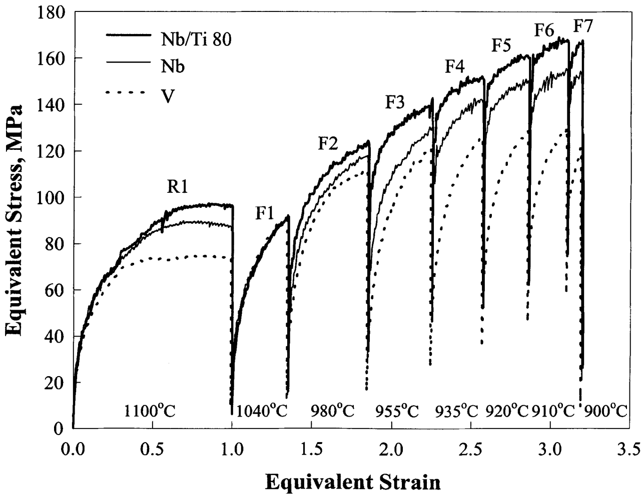

Fig. 1—Comparison of the hot deformation response from torsion tests for three classes of HSLA steels.

can only be fulfilled in the initial stands of the roughing mill, where temperatures are comparatively high, strain rates are relatively low, and reductions per pass are high. For the later roughing stands, and, in particular, during finish rolling, static recrystallization dominates.

B. *Recrystallization Kinetics*

An excellent overview of the general features of microstructural development during the actual rolling steps can be obtained from torsion simulations. Figure 1 shows the stress-strain curves of three of the five investigated steel grades; *i.e.,* V, Nb, and Nb/Ti 80. These three HSLA steels represent three distinct responses to the torsional simulation. Each simulation involves reheating at 1200 °C, one roughing pass, and seven finishing passes, all executed at a strain rate of 1/s, with interpass times between the finishing stands decreasing from 8 to 1 seconds. A constant low strain rate and somewhat larger-than-industrial interstand times were chosen for better control of the deformation temperature, which is indicated for each pass in Figure 1. However, it is important to note that more-accurate simulations of actual rolling schedules gave similar results, and the microstructures and properties produced matched those obtained under industrial rolling conditions.[33,38] The stress-strain curves of Figure 1 confirm clearly the capacity for Nb to retard recrystallization. In the Nb/Ti 80 steel with 0.086 wt pct Nb, no significant recrystallization takes place in the finishing passes, except after the first pass. For the Nb steel with 0.036 wt pct Nb, the accumulation of strain starts later, with the third finishing pass. No strain accumulation is seen to occur in the Nb-free V steel; *i.e.,* complete recrystallization is evident after each interstand time throughout the entire finishing-mill schedule, similar to that observed for plain carbon steels. In fact, the V steel behaves essentially like the DQSK steel, except that some precipitation strengthening is obtained during coiling, as discussed elsewhere in more detail.[39] The no-recrystallization temperatures concluded from the torsion tests are approximately 970 °C for the Nb/Ti 80 steel, 930 °C for the Nb steel, and 910 °C for the Nb/Ti 50 steel.

A more-detailed quantification of the recrystallization behavior was carried out using double-hit tests which emphasize static recrystallization, the dominant recrystallization mode obtained during finish rolling. This processing stage also determines the austenite microstructure entering the run-out table. The results further confirm the recrystallization tendencies concluded from the torsion tests. For the Nb-containing steels, there is clear evidence of strain retention from deformation below the no-recrystallization temperature (T_{nr}), as seen by the characteristic plateaus in the recrystallization curves occurring below approximately 1000 °C.[40] The plateau times can clearly be correlated with the precipitation start and finish times observed in stress-relaxation tests. However, as will subsequently be discussed in more detail, strain-induced precipitation is unlikely to occur in the finishing mill with mill residence times of not more than 10 seconds. But, even in the absence of precipitation, decreasing rates of static recrystallization are observed as the Nb content increases. Consequently, recrystallization appears to be solute drag–controlled for the hot-strip mill processing conditions.

In this case, the kinetics of static recrystallization can be characterized using an Avrami equation,[28,40] as proposed for plain carbon steels, in terms of the time for 50 pct recrystallization ($t_{0.5}$)

$$F_X = 1 - \exp\left(-0.693(t/t_{0.5})^k\right) \qquad [3]$$

where F_x is the fraction recrystallized and k is the Avrami exponent. The time for 50 pct recrystallization is a function of the applied strain (ε), the strain rate ($\dot{\varepsilon}$), the mean initial austenite grain size, and the deformation temperature (T), as follows:

$$t_{0.5} = A d_0\, \varepsilon^{-\beta}\, \dot{\varepsilon}^{-1/3} \exp\left(\frac{Q_{\text{rex}}}{\text{R}T}\right) \qquad [4]$$

where R is the gas constant and the parameters A, β, Q_{rex}, and k (from Eq. [3]) are summarized in Table VI. Figure 2 compares the static recrystallization kinetics exhibited by three steels to different Nb contents for typical processing parameters obtained in the last stands of the finishing mill. As illustrated, the recrystallization rates decrease with increasing Nb content because of increased solute drag. In Nb-free steels (DQSK and V), 90 pct recrystallization is attained in about 1 second. Thus, both steels will leave the finishing mill fully recrystallized. In the Nb-containing steels, the lower recrystallization rates lead to incomplete recrystallization and accumulation of retained strain (ε_r) in the finishing stands, as verified in the torsion tests (*cf.* Figure 1).

C. *Austenite Grain Size*

An important feature of the resulting austenite microstructure is the grain size. As long as recrystallization is complete, repeated grain refinement can be obtained from stand to stand, with the recrystallized grain size given by

$$d_{\text{rex}} = \Lambda d_0^{1/3}\, \varepsilon^{-p} \exp\left(-Q_{gx}/\text{R}T\right) \text{ for } d_{\text{rex}} > d_0 \qquad [5]$$

where the parameters Λ, p, and Q_{gx} are summarized in Table VI. A grain-size limit is attained when d_{rex} approaches the initial austenite grain size; *i.e.*, $d_{\text{rex}} = d_0$ for all cases where Eq. [5] would predict $d_{\text{rex}} < d_0$. The statically recrystallized

Table VI. Parameters Describing Static Recrystallization

Steel	k	A (s)	β	Q_{rex} (kJ/mol)	$\lambda(\mu m^{2/3})$	p	Q_{gx} (kJ/mol)
DQSK	2	4.35×10^{-13}	0.68	248	100	0.37	28
V	0.5	4.29×10^{-15}	2.0	262	100	0.37	28
Nb	0.5	4.10×10^{-17}	2.0	338	1.36×10^4	0.79	88
Nb/Ti 50	0.77	1.52×10^{-14}	1.5	275	1.36×10^4	0.79	88
Nb/Ti 80	1.32	7.25×10^{-18}	2.8	349	470	0.65	46
		($T > 1120$ °C)		($T > 1120$ °C)			
		1.00×10^{-12}		216			
		($T < 1120$ °C)		($T < 1120$ °C)			

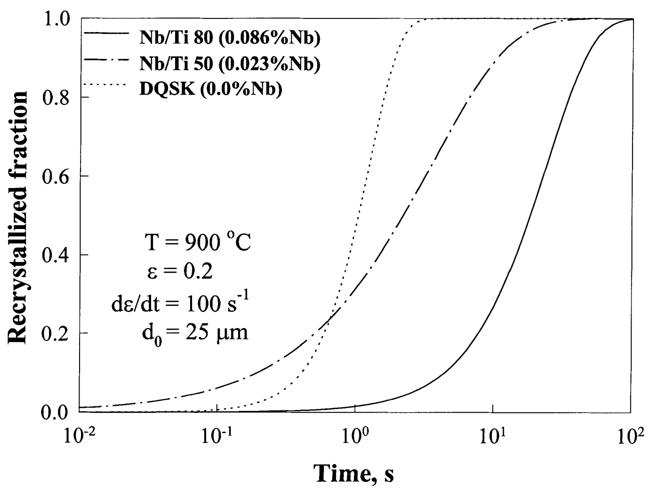

Fig. 2—Comparison of the predicted static recrystallization kinetics for steels with different Nb contents for typical conditions in the later finish stands with a rolling temperature of 900 °C, a strain of 0.2 at a strain rate of 100 s^{-1}, and an initial austenite grain size of 25 μm.

grain size decreases with increasing strain, decreasing initial austenite grain size, and decreasing temperature; the strain rate does not markedly affect the grain size produced by static recrystallization. The more-extensive grain refinement obtained at lower temperatures can be attributed to the reduced recovery and the associated increased dislocation density, which enhances the driving force for nucleation of recrystallized grains. It also reflects the lower mobility of recrystallizing grain boundaries resulting in lower growth rates, thereby allowing for a comparatively longer period for additional nucleation. Larger deformation (strain) generates a higher dislocation density and introduces smaller subgrains, thus increasing the density of nucleation sites for static recrystallization, which results in finer new grains. The effect of initial austenite grain size can be rationalized, assuming that the predominant nucleation occurs at grain boundaries and that the nucleation rate per boundary area is independent of grain size. These assumptions suggest a grain-size exponent of 1/3, in good agreement with empirical-fit values.[41] Consequently, larger initial grains are better relative grain refiners than smaller grains. A grain-refinement limit is attained when $d_{rex} = d_0$. Under industrial rolling conditions, this limit usually falls in the range from 20 to 40 μm, with the finer grains being obtained in the Nb-microalloyed steels.

As described in a previous article,[29] grain growth following recrystallization occurs unpinned in plain carbon steels, since AlN precipitation does not take place in austenite during industrial processing. This conclusion remains valid for the V steel, since V precipitates will not form during austenite rolling. In these steels, austenite grain growth is significant during the longer times between roughing stands and can be neglected during the small interpass times, decreasing from 4 to 0.5 seconds in finish rolling, in combination with comparatively low temperatures (900 °C to 1100 °C).[29,41] The situation is more complex when Nb and/or Ti are added to the steels. Since TiN does not dissolve during reheating, it is usually assumed that it provides sufficient pinning to prevent any significant austenite grain growth in Ti-microalloyed steels. However, the current grain-growth studies suggest that TiN particles may be coarse enough to have limited effectiveness in pinning grain boundaries.[37] For example, in the Nb/Ti 80 steel, TiN precipitates are observed, with sizes on the order of 1 μm, and substantial grain growth occurs with no apparent limit at temperatures above 1200 °C, as evident from Table IV. However, austenite grain-growth inhibition is confirmed for much-finer TiN distributions, as found in the lower-Ti-grade Nb/Ti 50, where holding at 1200 °C does result in the same grain size as that observed at 1100 °C and 1150 °C, respectively.[37] Since the particle-size distribution of TiN results essentially from casting,[42] it is likely that the effectiveness of grain-boundary pinning due to Ti additions is fixed before the slabs are reheated in a hot-strip mill. Thus, the TiN distribution could be considered to be an additional parameter to the steel chemistry which affects the microstructure-property evolution. However, the overall significance of this variable is thought to be minor. In addition, for the overall austenite grain-size evolution, the effects of Nb have to be considered. Having seen the considerable solute-drag effect of Nb on recrystallization, the solute Nb must have an even more pronounced effect on grain growth, with its much lower driving pressures, than on recrystallization. Even in cases with no Ti additions or ineffective TiN pinning, Nb solute drag prevents significant austenite grain growth at temperatures well in excess of the no-recrystallization temperature. An exact quantification of the Nb solute-drag effect on austenite grain growth requires additional studies; the current results are not conclusive.[37] However, as is the case for plain carbon steels, the austenite grain size at the exit of the finishing mill is primarily given by the recrystallized grain size and is little affected by grain growth at the lower finishing temperatures and shorter interstand times; this would also be expected to be true for the microalloyed steels.

IV. AUSTENITE-TO-FERRITE TRANSFORMATION AND FERRITE GRAIN SIZE

A. *Austenite Decomposition Kinetics*

The CCT tests on undeformed samples reveal similar tendencies for all five steel grades investigated. Increasing the cooling rate and/or increasing the austenite grain size lowers the transformation temperature. In particular, for the higher-alloyed grades (*e.g.*, Nb/Ti 80), this is also associated with a considerable tendency to form acicular microstructures. For the Nb-containing steels, it is necessary to evaluate the effect of a pancaked austenite microstructure on the transformation kinetics, thereby incorporating the effect of controlled rolling into the transformation studies. Surprisingly, there is little effect of a deformed austenite microstructure on the transformation behavior under accelerated cooling conditions, as discussed in detail elsewhere for the Nb steel.[43] The major effect of retained strain is to encourage the production of a predominantly polygonal ferrite microstructure. This becomes a critical issue for the Nb/Ti 80 steel, where, because of its higher Mn content, without retained strain, a very fine austenite microstructure with grain sizes of approximately 10 μm is required to produce a polygonal ferrite microstructure by accelerated cooling conditions. For larger austenite grains, the presence of a retained strain of approximately 0.6 or more, which can be expected to be the accumulated strain during controlled rolling of this grade, is a prerequisite to form a polygonal ferrite microstructure. Figure 3 shows examples of the ferrite microstructures obtained for all five grades in the CCT tests, having cooling rates of approximately 100 °C/s and initial austenite microstructures similar to those expected at the exit of the finish mill. All five steels exhibit a ferrite microstructure. As the transformation temperatures decrease, the ferrite grain sizes decrease and there is also a tendency to form less and less polygonal ferrite, albeit the determination of the ferrite grain size is still possible for the quasi-polygonal ferrite of the Nb/Ti 80 steel.

One of the compromises of the Gleeble tests is that controlling the austenite grain size by reheating does not exactly duplicate the precipitation state that would be relevant for the hot-strip mill. In particular, for the finer austenite microstructures, the reheating temperatures are too low to obtain significant dissolution of those carbides and nitrides; *i.e.*, VC, VN, TiC, NbC, and NbN, which would dissolve during reheating in the mill. For this reason, the CCT microstructures are also compared to those obtained by torsion testing, where the mill conditions are more closely simulated. No significantly different ferrite grain sizes are found except for the V steel, where the ferrite grain sizes appear to consistently be 25 pct larger in the torsion samples than in those obtained in CCT tests. Thus, it was concluded that, at least as a first approximation, the potential solute-drag effects of the microalloying elements on the austenite-to-ferrite transformation do not have to be assessed specifically. With this recognized limitation, the plain low-carbon steel model previously developed to describe the transformation kinetics on the run-out table can be used to describe the transformation kinetics of HSLA steels as well.[30,31]

The transformation start temperature (T_s), which can be associated with nucleation-site saturation at austenite grain boundaries, is predicted, assuming the early growth of corner ferrite nucleated at T_N to be rate controlling (Table VII), *i.e.*,[30]

$$\frac{dR_f}{dT}\frac{dT}{dt} = D_C \frac{c_\gamma - c^0}{c_\gamma - c_\alpha}\frac{1}{R_f} \quad [6]$$

where R_f is the radius of the growing ferrite grain, D_C is the carbon diffusivity in austenite,[44] c^0 is the average carbon bulk concentration and c_α and c_γ are the equilibrium carbon concentrations in ferrite and austenite, respectively. The condition for nucleation-site saturation is reached if

$$R_f \geq \frac{(c^* - c^0)}{(c_\gamma - c^0)}\frac{d_\gamma}{\sqrt{2}} \quad [7]$$

where d_γ is the austenite grain size and c^* indicates a limiting carbon concentration in the vicinity of the growing ferrite nuclei, above which ferrite nucleation is inhibited. For a constant cooling rate (φ), Eqs. [6] and [7] lead to

$$c^* - c^0 = \frac{2(c_\gamma - c^0)}{\varphi^{1/2}\, d_\gamma}\sqrt{\int_{T_S}^{T_N} D_C \frac{c_\gamma - c^0}{c_\gamma - c_\alpha}\, dT} \quad [8]$$

which suggests that the transformation start temperature is a function of cooling rate and grain-boundary area; *i.e.*, $\varphi\, d_\gamma^2$. As a first approximation, c^* can be taken as a constant, as shown in Figure 4 for the Nb steel, where $c^* = 1.3\, c^0$, similar to that used for the DQSK and V steel values.[31] Figure 4 also illustrates that, for accelerated cooling conditions, the effect of retained strain on the transformation start can be neglected for this steel grade. However, in the Nb/Ti 80 steel, a small but marked effect of retained strain is evident. The c^* value decreases from 2.2 to 2.0 c^0 as the retained strain increases from 0 to 0.6, reflecting an increase of the transformation temperature by approximately 20 °C due to a pancaked austenite microstructure. A more-striking effect is obvious when the c^*/c^0 ratios (1.3 for the Nb steel and 2.0 for the controlled-rolled Nb/Ti 80 steel) for both grades are being compared, as illustrated in Figure 5. A larger c^*/c^0 ratio, which is associated with a higher undercooling to attain transformation start for the same combined cooling/grain-size condition, indicates a significantly larger solute drag–like effect at the moving α-γ interface. The latter can primarily be attributed to Mn, as the c^*/c^0 ratio increases from 1.3 with 0.48 wt pct Mn to 2.0 with 1.35 wt pct Mn. In addition to Mn, the increased Nb content in the Nb/Ti 80 grade (0.086 wt pct) compared to that in the Nb grade (0.036 wt pct) may also enhance the solute drag–like effect, as suggested by Subramanian *et al.*[45] To improve the accuracy for predicting the onset of the phase transformation, c^* may be represented as[43]

$$c^* = (x^* + x_\gamma/d_\gamma + \Delta x \exp(-0.0003(T_N - T)^{2.2})\, c^0 \quad [9]$$

where the parameters x^*, x_γ, and Δx are summarized in Table VII.

The subsequent ferrite growth can be described using an Avrami approach and adopting additivity. The ferrite fraction (X) transformed at $T = T(t)$ can be written as[46]

$$X = \frac{c_\gamma - c^0}{c_\gamma - c_\alpha}\left(1 - \exp\left(\frac{1}{d_\gamma^m}\left(\int_{T_S}^{T}\frac{\exp((b_1(T_{\mathrm{Ae3}} - T') + b_2)/n)}{\varphi(T')}\, dT'\right)^n\right)\right) \quad [10]$$

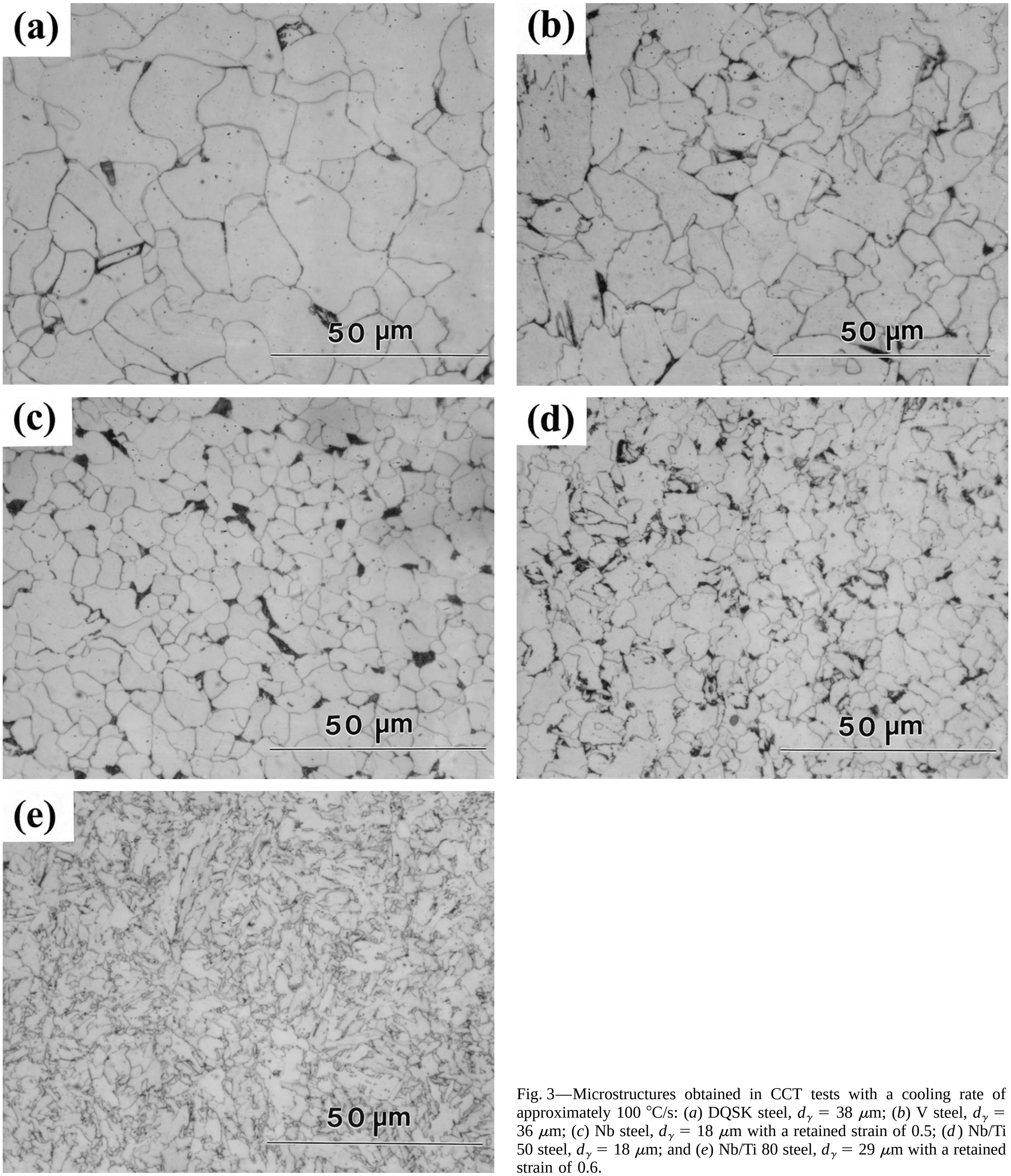

Fig. 3—Microstructures obtained in CCT tests with a cooling rate of approximately 100 °C/s: (*a*) DQSK steel, $d_\gamma = 38$ μm; (*b*) V steel, $d_\gamma = 36$ μm; (*c*) Nb steel, $d_\gamma = 18$ μm with a retained strain of 0.5; (*d*) Nb/Ti 50 steel, $d_\gamma = 18$ μm; and (*e*) Nb/Ti 80 steel, $d_\gamma = 29$ μm with a retained strain of 0.6.

where $\varphi(T) = -dT/dt$ is the instantaneous cooling rate, and b_1, b_2, and m are summarized in Table VII. The Avrami exponent, $n = 0.9$, can be used for all steel grades studied; *i.e.*, the findings for the plain carbon steels[31,35] remain valid for the HSLA steels as well. An Avrami exponent of approximately 1, which was also reported for a variety of other plain carbon steels,[47] indicates nucleation-site saturation and one-dimensional ferrite growth from austenite grain boundaries.

In general, a ferrite fraction of 95 pct or more is formed under industrial hot rolling, controlled cooling, and coiling conditions for the low-carbon steels investigated in this study. However, the potential for forming nonferritic transformation products has to be considered for the Nb/Ti 80 grade; although retained strain extends the cooling-rate range for which polygonal (or quasi-polygonal) ferrite is being formed, nonpolygonal or acicular ferrite is present. However, a detailed quantification of the amount of nonpolygonal

Table VII. Parameters Describing Austenite-to-Ferrite Transformation and Ferrite Grain Size

Steel	T_N, °C	x^*	x_γ	Δx	m	b_1 (1/°C)	b_2	Ξ (μm^{-q})	q
DQSK	843	1.15	9.1	0.15	2.2	0.033	4.8	50.7	0.024
V	843	1.18	4.2	0.15	1.8	0.022	4.2	47.3	0.037
Nb	805	1.14	4.6	0.15	1.8	0.030	1.1	49.6	0.036
Nb/Ti 50	800	1.23	8.5	0.15	1.3	0.026	−0.44	50.7	0.037
Nb/Ti 80*	785	2.00	0	0	1.3	0.035	−3.6	**	**

*Controlled rolled with $\varepsilon_r \geq 0.6$.
**No grain size dependence recorded.

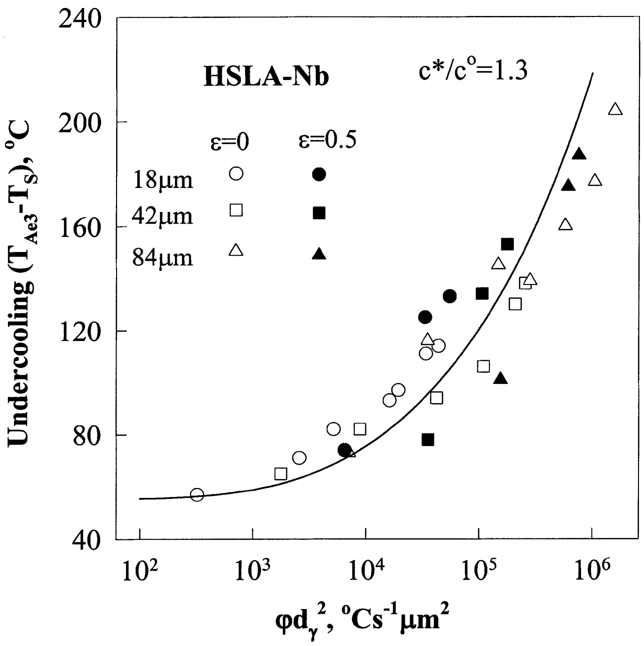

Fig. 4—Effect of retained strain on the transformation start temperature, T_S, in the Nb steel as a function of cooling rate, φ, and austenite grain size, d_γ.[43]

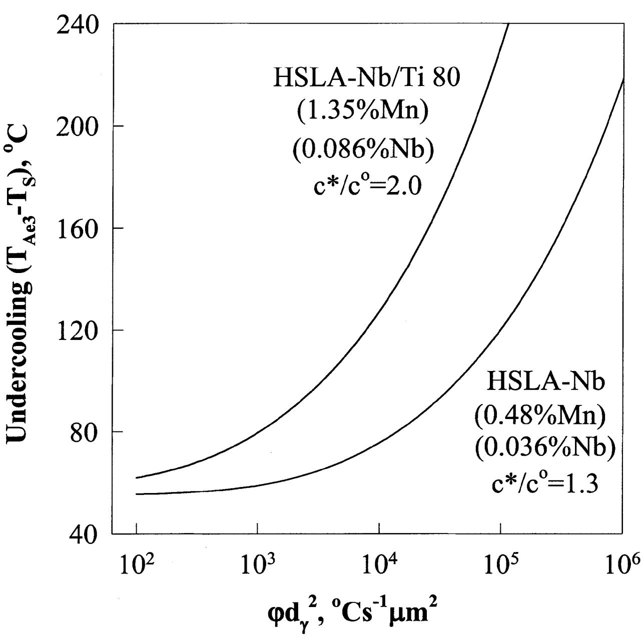

Fig. 5—Effect of Mn and Nb on the degree of undercooling, $\Delta T = T_{Ae_3} - T_S$, required for the transformation start.

ferrite formed is difficult, and only estimates can currently be made to characterize the transition condition contributing to the formation of nonpolygonal structures. Unfortunately, adopting a critical α-γ interface velocity to indicate the ferrite stop condition, as proposed for plain carbon steels,[31,48] cannot be extended to HSLA steels. An alternative approach incorporating the effect of retained strain has been adopted, where

$$T_{\text{transition}} = 620 - 600\varepsilon_r^3 \text{ (in °C) (for } \varepsilon_r < 0.6) \quad [11a]$$

and

$$T_{\text{transition}} = 490 \text{ (in °C) (for } \varepsilon_r > 0.6) \quad [11b]$$

is the temperature below which nonpolygonal transformation products start to form in the Nb/Ti 80 steel.

B. *Ferrite Grain Size*

The ferrite grain size results from austenite decomposition; no significant ferrite grain growth takes place for coiling temperatures below 700 °C. The CCT results indicate that the ferrite grain size (d_α) can be expressed as a function of the transformation start temperature in the form suggested by Suehiro *et al.*,[49]

$$d_\alpha = (F \exp (B - E/T_S))^{1/3} \quad [12]$$

where d_α is the EQAD in micrometers; T_S is in Kelvin; F is the final ferrite fraction; $E = 51{,}000$ for all steels but the Nb/Ti 80 grade, where $E = 15{,}400$; and B is a function of the initial austenite microstructure. In the absence of retained strain, B can be expressed as

$$B = \Xi d_\gamma^q \quad [13]$$

with the parameters Ξ and q being summarized in Table VII. Figure 6 shows the correlation of the ferrite grain size and the transformation start temperature determined in CCT tests without deformation for the medium-strength HSLA steels.

In the Nb-microalloyed steels, the effect of retained strain has to be incorporated before the model can be applied to controlled rolling. For the lowest Nb grade, Nb/Ti 50, these effects are negligible. As shown elsewhere,[43] a limiting ferrite grain size($d_{\alpha\text{lim}}$) is approached in the Nb steel as ε_r increases. This can be reflected in the combined transformation–ferrite-grain-size model by adopting an effective austenite grain size of $d^* = 10$ μm, for $\varepsilon_r \geq 0.5$, to predict the ferrite grain size; a linear interpolation between the strain-free case and $d_{\alpha\text{lim}}$ is suggested for intermediate strain levels. In the Nb/Ti 80 steel, where the effects of retained strain are more pronounced, B may be written as a function of the retained strain rather than the austenite grain size:[38]

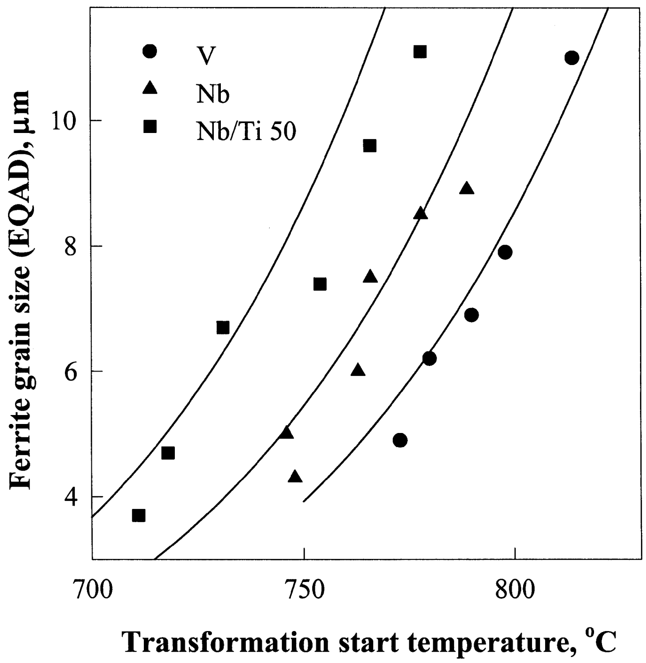

Fig. 6—Ferrite grain size as a function of the transformation start temperature for the medium strength HSLA steels, as obtained in the CCT tests without deformation after reheating at 950 °C; the solid lines indicate predictions.

$$B = 19.5 + 1.7 \exp(-6\varepsilon_r) \quad [14]$$

To relate the ferrite grain size to the early transformation is consistent with the findings of Priestner and Hodgson.[50] With in-depth studies, they showed that the ferrite grain size is determined by the nucleation and the early growth processes of the ferrite. An important implication of Eq. [12] is that designing the run-out table cooling pattern before and in the initial stages of the transformation is critical to maximize the effects of accelerated cooling on the ferrite grain refinement. Cooling is less critical once the transformation is initiated, except, perhaps, for the Nb/Ti 80 steel, where too-rapid cooling during transformation may trigger the development of nonpolygonal transformation products. Pereloma and Boyd[51] addressed this issue by investigating stepped cooling regimes. Additional work using similar tests is required to refine the ferrite-grain-size and transformation model for the Nb/Ti 80 grade.

Figure 7 compares the predicted ferrite grain size for three HSLA steels as a function of the average cooling rate, from T_N to T_S. The austenite microstructure produced during finish rolling is approximated by $d_\gamma = 30$ μm and $\varepsilon_r = 0.6$ for the Nb/Ti 80 grade, $d_\gamma = 20$ μm and $\varepsilon_r = 0.5$ for the Nb grade, and $d_\gamma = 30$ μm for the V steel. The predicted ferrite grain size for the V steel is obtained by multiplying the d_α relationship concluded from the CCT tests by a factor of 1.25 to reflect the anticipated role of solute V under industrial conditions. Clearly, the beneficial effect of accelerated cooling on ferrite grain refinement is evident. Changing d_γ, in the range from 20 to 40 μm, appears of minor importance for the fully recrystallized steels, with the resulting d_α varying on the order of 10 to 15 pct.[52] Further, in the Nb-microalloyed steels, the amount of retained strain does mask the effect of the actual austenite grain size (*cf., e.g.*, Eq. [14]). The cooling rates in the water-spray zones of a run-out table, where the

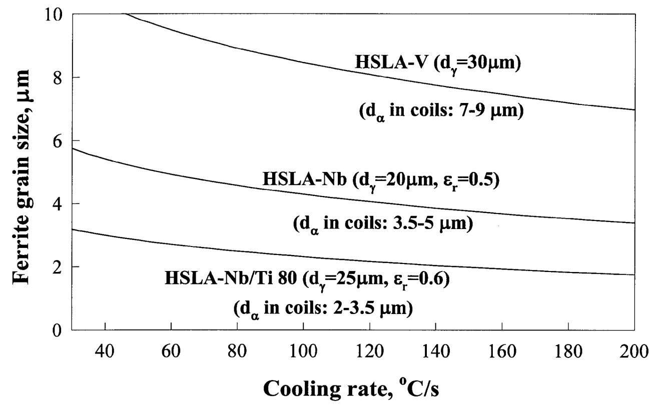

Fig. 7—Ferrite grain size predictions for three classes of HSLA steels.

ferrite transformation initiates, are usually in the range from 100 °C/s to 150 °C/s, depending on the strip thickness and velocity. The results shown in Figure 7 suggest a ferrite grain size of approximately 8 μm for the HSLA-V steel, 4 μm for the controlled-rolled HSLA-Nb steel, and 2.5 μm for the controlled-rolled Nb/Ti 80 steel. These predictions are in good agreement with measurements made on hot-rolled coil samples having a ferrite grain size ranging from 7 to 9 μm for the V steel, from 3.5 to 5 μm for the Nb steel, and from 2 to 3 μm for the Nb/Ti 80 steel.

V. PRECIPITATION

A. *Strain-Induced Precipitation in Austenite*

The study of strain-induced precipitation in austenite emphasized the Nb-containing steels, in particular, those with a higher Nb content; *i.e.*, the Nb and the Nb/Ti 80 steels. The precipitation kinetics in austenite were investigated with a stress-relaxation technique, where two characteristic inflection points in the stress-relaxation curves indicate the precipitation start time (P_s) and the precipitation finish time (P_f).[16,34] The complexity of this method requires deformation conditions (10 pct strain at a strain rate of 0.1 s^{-1}) which are far from those of hot rolling. However, the relevance of these measurements has been confirmed with double-hit tests at higher strains and strain rates, where characteristic plateaus in the softening behavior are observed at similar times for a given temperature.[40] The P_s and P_f values measured at different test temperatures in the stress-relaxation tests were used to construct the precipitation-time-temperature (PTT) diagram shown in Figure 8. The TEM analysis of replicas confirmed the presence of Nb particles in the Nb steel, as well as TiN, and more-complex Nb and Ti precipitates in the Nb/Ti 80 steel. TiN is a stable precipitate which does not dissolve during reheating. Based on these observations, it was concluded that strain-induced precipitation of Nb(CN) can occur in the Nb steel and of NbC, as well as TiC and/or (Nb,Ti)C, in the Nb/Ti 80 steel.

As shown in Figure 8, an earlier precipitation start is observed for the Nb steel, this grade having less Nb (0.036 wt pct) than the Nb/Ti 80 grade (0.086 wt pct.). This is attributed to the precipitation of carbonitrides in the Nb grade, whereas, in the higher-Nb grade (Nb/Ti80), all of the N is tied up in TiN and only carbides can form. The carbides show lower nucleation rates, consistent with estimates of

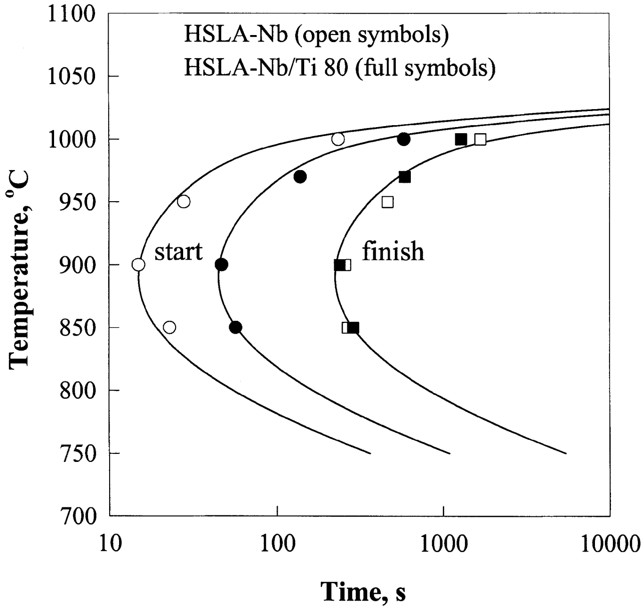

Fig. 8—Precipitation-time-temperature diagram for the HSLA-Nb and HSLA-Nb/Ti 80 grades.

interfacial energies by Sun *et al.*[14] More important, the measured precipitation start times exceed, in both grades, the finish mill residence times. Thus, to a first approximation, it is assumed that all Nb (and excess Ti) remains in solution after finish rolling in a hot-strip mill. However, Nb(CN) or (Nb,Ti)C precipitation is predicted for the extended processing times experienced in a Steckel mill. Significant precipitation may occur in a Steckel mill, with the degree of precipitation strengthening being a function of the rolling temperature and the mill residence time, as discussed by Collins *et al.*[53] To extend the present model to these different processing conditions, further studies of the precipitation detail are required to develop a kinetic model, for example, one similar to that proposed by Sun *et al.*[20]

B. *Precipitation in Ferrite*

In a hot-strip mill, the precipitation of the various carbides and nitrides occurs primarily in ferrite during coiling, with the exception of the TiN, which is formed near the melting temperature and is stable throughout the entire rolling process. In Al-killed plain carbon steel, precipitation is related to the formation of AlN. This precipitation process does not provide significant hardening, as do the carbides and nitrides in the microalloyed grades. Nevertheless, the status of AlN precipitation in the hot band is of practical importance, since it controls texture development during subsequent cold rolling and annealing, thereby affecting the formability characteristics of the steel sheet. The kinetics of AlN precipitation in hot-rolled DQSK coils can be described by the model of Duit *et al.*[54] The amount of nitrogen in solution is given by

$$N_{\text{free}} = N_{\text{total}} - 5190\ \text{Al}_{as}\left(1 - \exp\left(-\left(\int_{t_0}^{t} \frac{\exp\left(-260\ \text{kJmol}^{-1}/\text{R}T\right)}{4.3 \times 10^{-10}\ \text{s}}\right)^{0.44}\right)\right) \qquad [15]$$

where N_{total} is the total amount of nitrogen (in parts per million), and Al_{as} is the amount of acid-soluble aluminum (in weight percent). Equation [15] was developed for the following chemistry range: 15 ppm $< N_{\text{total}} <$ 75 ppm and 0.028 wt pct $< \text{Al}_{as} <$ 0.0052 wt pct.

For the HSLA steels, aging tests in combination with hardness measurements provide information on the extent of precipitate strengthening and, at least indirectly, also on the precipitation kinetics. Extensive TEM work is needed to obtain the actual data describing the development of the precipitate population. Aging tests were carried out on torsion samples (Nb-containing steels) or, when available, on rapidly cooled tail pieces of a coil (V steel). The development of an aging peak, where peak times increase as aging temperature decreases, are observed for both the V steel[55] and the Nb/Ti 80 steel, which has the highest Nb content. For the lower-Nb grades, only overaging with an associated decreasing hardness could be verified. For a given steel grade, the peak hardness is independent of the aging temperature, suggesting a temperature-independent volume fraction of strengthening precipitates. This is consistent with the extremely low solubility of all microalloying elements in ferrite. Moreover, TEM investigations clearly confirmed particle coarsening to be responsible for the observed aging behavior.[55]

Assuming that coarsening of V(CN) and Nb(CN) is the relevant rate-controlling step of the precipitation kinetics, the mean particle size (r) can be determined, according to the Lifshitz–Slyozov–Wagner theory, to be[56,57]

$$r^3 - r_0^3 = Ct \exp\left(-Q/\text{R}T\right)/T \qquad [16]$$

where r_0 is the initial mean particle size, C a constant, and Q is the effective activation energy of bulk diffusion of V and Nb. Based on Eq. [16], a temperature-corrected time, (P)[58]

$$P = \frac{t \exp\left(-Q/\text{R}T\right)}{T} \qquad [17]$$

can be introduced to characterize precipitation during aging. Precipitation strengthening ($\Delta\sigma$) is a function of P, with the maximum or peak strength being realized at P_p. Master curves for precipitation age hardening can be constructed by introducing a normalized temperature-corrected time ($P^* = P/P_p$) and a normalized precipitation-strength contribution ($\Delta\sigma/\Delta\sigma_p$), where $\Delta\sigma_p$ is the peak-strength contribution. Figure 9 compares the normalized hardness changes observed in the Nb/Ti 80 steel to those obtained for a 0.046 wt pct Nb steel, as reported by Vollrath *et at.*[59] At least to a first approximation, the precipitation-strengthening kinetics of both steels can be described with the same parameters, based on the following relationship:[55,58]

$$\Delta\sigma = \frac{1.9\Delta\sigma_p(P^*/4)^{1/6}}{1 + (P^*/4)^{1/2}} \qquad [18]$$

which assumes that the base strength, related to ferrite grain size and ferrite fraction, can be described by the structure-property relations proposed for plain carbon steels by Choquet *et al.*[2] The initial part of the aging curve, *i.e.*, $P^* < 0.001$, is also affected by solute solution strengthening because of incomplete precipitation.[55] It can be concluded that, in both steels, Nb diffusion is rate limiting for precipitation strengthening, and other effects, like interparticle spacing or Ti diffusion (approximately 20 pct of the precipitation

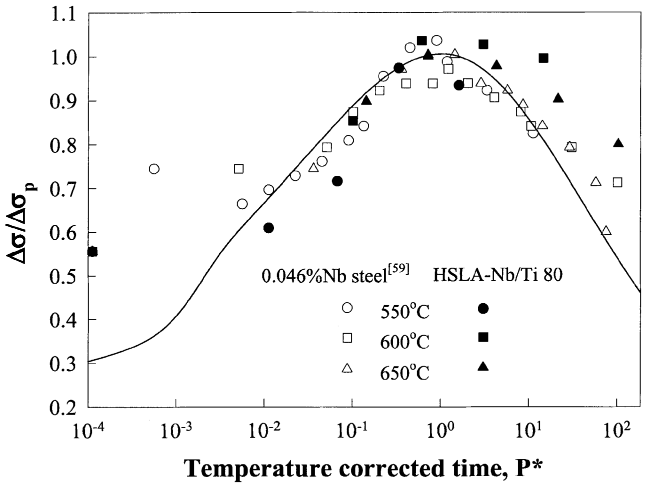

Fig. 9—Precipitation hardening in Nb-containing HSLA steels; open symbols represent the results of Vollrath *et al.*[59] for a 0.046 pct Nb steel, full symbols those of this study for the HSLA-Nb/Ti 80 steel, and the solid line indicates the prediction.

strengthening in the Nb/Ti 80 steel can be attributed to TiC), are of second order. This analysis can also be applied to the V steel. As a result, the parameters Q and P_p can be attributed to the major microalloying element, *i.e.*, V and Nb, respectively, with $Q = 384$ kJ/mol and $P_p = 1.3 \times 10^{-21}$ s/K being adopted for the V steel and $Q = 269$ kJ/mol and $P_p = 4.7 \times 10^{-16}$ s/K being adopted for the Nb-microalloyed steels.[55] It is also apparent that the aging curves exhibit a fairly broad peak. As can be seen in Figure 9, approximately 90 pct of the peak strength is realized, even though aging times are as much as one order of magnitude larger or smaller than the actual peak aging time.

To appreciate the precipitation strength developed during coil cooling, Eq. [17] can be written as

$$P = \int_{t_0}^{t} \frac{\exp\,(-\,Q/RT(t'))}{T(t')}\,dt' \qquad [19]$$

to incorporate temperature changes with time. Figure 10 shows the normalized precipitation-strength contribution as a function of coiling temperatures for both V-and Nb-microalloyed steels, assuming coil cooling at a rate of 30 °C/h. The results suggest that V steels should be coiled at 635 °C to 720 °C, and Nb steels at 570 °C to 675 °C, to develop at least 90 pct of their precipitation-strength potential, with the maximum precipitation strength for each steel being observed at approximately 675 °C and 625 °C, respectively. These predictions are consistent with industrial coiling practices for these steel grades.

Unlike the relative precipitation strength, the maximum precipitation-strength contribution does strongly depend on the microalloy content. In general, there is an increase in strength as the microalloy addition increases.[60] Table VIII summarizes the $\Delta\sigma_p$ values of the four HSLA steels examined in this study. Additional research is required to develop chemistry-sensitive relations for the precipitation-strengthening potential. This would be a prerequisite to extending the current microstructural model to Steckel mill operations, where, depending on the mill residence time, only a fraction of the microalloy addition remains in solution after rolling and can contribute to precipitation strength.

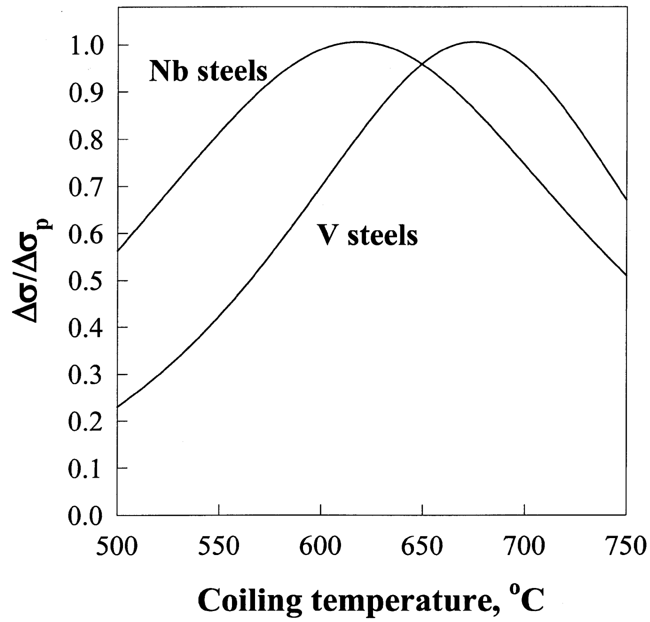

Fig. 10—Prediction of normalized precipitation strength as a function of coiling temperature when a 30 °C/h cooling is assumed to characterize coiling.

Table VIII. Maximum Precipitation Strength Contribution (MPa)

Steel	V	Nb	Nb/Ti 50	Nb/Ti 80
$\Delta\sigma_p$	145	152	126	225

VI. CONCLUSIONS

A comprehensive microstructural model has been developed for hot-strip rolling of microalloyed, low-carbon steels. The model addresses recrystallization kinetics during finish rolling, the ferrite grain size resulting from the austenite-to-ferrite transformation on the run-out table, and precipitation of carbides, nitrides, and/or carbonitrides during coiling as the key features affecting the desired properties of the hot-rolled steel. The microstructural model has been incorporated into a state-of-the-art temperature-and-deformation process model. Predictions from this model for industrial processing have been reported for plain carbon steels, including DQSK steel.[7,61,62] The model has also been modified to incorporate HSLA steels.[38] Validation of the process model for HSLA steels is currently being performed in cooperation with a number of steel companies across North America.

Process models which draw on fundamentally based comprehensive microstructural models, similar to that presented here, appear to be promising tools which may aid the steel industry in producing high-quality hot bands with tight property tolerances. The current models appear to be reliable for medium-strength HSLA steels; *i.e.*, steels like the V, Nb, and Nb/Ti50 steels of this study. Although the present model would benefit by incorporating the effect of steel chemistry, extensive laboratory work is still required to quantify the effect of chemistry variations. Moreover, additional work is essential in order to improve the quality of the model predictions for the higher-strength grades, like the Nb/Ti 80 steel. The probable future applicability of the process model will be for the advanced steel grades, such as the HSLA-80 steels. The modeling approach, which necessarily quantifies the metallurgical microstructural evolution mechanisms, should contribute to the development of even higher–strength HSLA steels for commercial applications, *e.g.*, for linepipe grades.[63] Thus, future work will be concentrated on these more-advanced steels, where the challenges are twofold.

First, the ferrite microstructure in these steels (*e.g.*, HSLA-80) displays visible deviation from the polygonal grain structure which is present in the lower-strength grades. This acicular ferrite, with a higher dislocation density and associated transformation hardening, requires a more detailed metallographic and microhardness characterization before adequate structure-property relationships can be proposed. In addition, unlike the grades with polygonal ferrite, the later transformation stages in these steels have to be quantified with more accuracy to better appreciate the mechanisms which develop the acicular transformation products. Further, these and similar studies are required to develop transformation models for hot-rolled multiphase steels displaying transformation-induced plasticity.

Second, there are limits to adequately simulating in the laboratory the precipitation and segregation behavior of the microalloying elements, which occurs during industrial rolling. Thus, microstructural models developed from laboratory simulation tests require critical assessment to evaluate their potential differences with respect to the particle-pinning and solute-drag forces that exist during industrial processing.

Despite these challenges, the proposed microstructural modeling approach is sufficiently general to be easily extended to compact strip production[64] and other advanced processing routes, which are currently under development in the steel industry.

ACKNOWLEDGMENTS

The authors acknowledge the financial support received from the American Iron and Steel Institute (AISI) and the United States Department of Energy (DOE). The steels were supplied by the Gary Works of U.S. Steel (Gary, IN), the Indiana Harbor Works of LTV Steel Company (Indiana Harbor, IN), and the Lake Erie Steel Co. Ltd., a subsidiary of Stelco Inc. (Nanticoke, ON). The authors are, in particular, grateful to W.P. Sun for his contributions to the recrystallization and precipitation investigations in the early part of this project. Discussions with I.V. Samarasekera and W.J. Poole throughout the project work are greatly appreciated. A. Giumelli and R. Pandi made significant contributions as graduate students in the areas of austenite grain growth and austenite decomposition, respectively. The able assistance of B. Chau, R. Cardeno, X. Chen, T. Cheng, S. Lechuk, and P. Wenman is acknowledged and was instrumental in conducting and analyzing the experiments.

REFERENCES

1. R.A. Heimbuch: *40th Mechanical Working and Steel Processing Conf. Proc.*, ISS, Warrendale, PA, 1998, vol. XXXVI, pp. 3-10.
2. P. Choquet, P. Fabregue, J. Giusti, B. Chamont, J.N. Pezant, and F. Blanchet: in *Mathematical Modelling of Hot Rolling of Steels*, S. Yue, ed., The Metallurgical Society of CIM, Montreal, pp. 34-43.
3. J.J. Jonas and C.M. Sellars: *Iron Steelmaker*, 1992, vol. 19(10), pp. 67-71.
4. P.D. Hodgson and R.K. Gibbs: *Iron Steel Inst. Jpn. Int.*, 1992, vol. 32, pp. 1329-38.
5. T. Senuma, M. Suehiro, and H. Yada: *Iron Steel Inst. Jpn. Int.*, 1992, vol. 32, pp. 423-32.
6. O. Kwon, K.J. Lee, J.K. Lee, K.B. Kang, J.K. Kim, J.D. Lee, and J. Kim: *HSLA Steels '95*, G. Liu, H. Stuart, H. Zhang, and C. Li, eds., China Science and Technology Press, Beijing, 1995, pp. 82-89.
7. D.Q. Jin, V.H. Hernandez-Avila, I.V. Samarasekera, and J.K. Brimacombe: *Modelling of Metal Rolling Processes*, The Institute of Materials, London, 1996, pp. 36-58.
8. J. Andorfer, D. Auzinger, B. Buchmayr, W. Giselbrecht, G. Hribernig, G. Hubmer, A. Luger, and A. Samoilov: *Thermec '97*, T. Chandra and T. Sakai, eds., TMS, Warrendale, PA, 1997, pp. 2069-75.
9. D.Q. Bai, S. Yue, W.P. Sun, and J.J. Jonas: *Metall. Trans. A*, 1993, vol. 24A, pp. 2151-59.
10. R.L. Bodnar, R.O. Adebanjo, and S.S. Hansen: *37th Mechanical Working and Steel Processing Conf. Proc.*, ISS, Warrendale, PA, 1995, vol. XXXIII, pp. 743-57.
11. T. Siwecki, B. Hutchinson, and S. Zajac: *Microalloying '95*, ISS, Warrendale, PA, 1995, pp. 197-211.
12. S.F. Medina: *Mater. Sci. Technol.*, 1998, vol. 14, pp. 217-21.
13. B. Dutta and C.M. Sellars: *Mater. Sci. Technol.*, 1987, vol. 3, pp. 197-206.
14. W.P. Sun, M. Militzer, and J.J. Jonas: *Can. Metall. Q.*, 1993, vol. 32, pp. 155-63.
15. H. Zou and J.S. Kirkaldy: *Metall. Trans. A*, 1991, vol. 22A, pp. 1511-24.
16. W.J. Liu and J.J. Jonas: *Metall. Trans. A*, 1988, vol. 19A, pp. 1403-13.
17. W.J. Liu: *Metall. Mater. Trans. A*, 1995, vol. 26A, pp. 1641-57.
18. S.P. Gupta: *Steel Res.*, 1993, vol. 64, pp. 623-29.
19. F. Ishikawa, T. Takahashi, and T. Ochi: *Metall. Mater. Trans. A*, 1994, vol. 25A, pp. 929-36.
20. W.P. Sun, M. Militzer, D.Q. Bai, and J.J. Jonas: *Acta Metall. Mater.*, 1993, vol. 41, pp. 3595-3604.
21. M. Djahazi, X.L. He, J.J. Jonas, and W.P. Sun: *Mater. Sci. Technol.*, 1992, vol. 8, pp. 628-35.
22. R.C. Peterson, B.A. Parker, and R.K. Gibbs: in *Low Carbon Steels for the 90's*, R. Asfahani and G. Tither, eds., TMS, Warrendale, PA, 1993, pp. 131-37.
23. Z. Yao: *High Strength Sheet Steels for the Automotive Industry*, ISS, Warrendale, PA, 1994, pp. 37-44.
24. J.J. Jonas and I. Weiss: *Met. Sci.*, 1979, vol. 13, pp. 238-45.
25. S. Yamamoto, C. Ouchi, and T. Osuka: in *Thermomechanical Processing of Microalloyed Austenite*, A.J. DeArdo, G.A. Ratz, and P.J. Wray, eds., AIME, Warrendale, PA, 1982, pp. 613-39.
26. X.L. He, M. Djahazi, J.J. Jonas, and J. Jackman: *Acta Metall. Mater.*, 1991, vol. 39, pp. 2295-2308.
27. N. Maruyama, R. Uemori, and M. Sugiyama: *Mater. Sci. Eng. A*, 1998, vol. A250, pp. 2-7.
28. W.P. Sun and E.B. Hawbolt: *Iron Steel Inst. Jpn. Int.* 1997, vol. 37, pp. 1000-09.
29. M. Militzer, A. Giumelli, E.B. Hawbolt, and T.R. Meadowcroft: *Metall. Mater. Trans. A*, 1996, vol. 27A, pp. 3399-3409.
30. M. Militzer, R. Pandi, and E.B. Hawbolt: *Metall. Mater. Trans. A*, 1996, vol 27A, pp. 1547-56.
31. M. Militzer, R. Pandi, E.B. Hawbolt, and T.R. Meadowcroft: in *Hot Workability of Steels and Light Alloys-Composites*, H.J. McQueen, E.V. Konopleva, and N.D. Ryan, eds., The Metallurgical Society of CIM, Montreal, 1996, pp. 373-80.
32. J.S. Kirkaldy and E.A. Baganis: *Metall. Trans. A*, 1978, vol. 9A, pp. 459-501.
33. D. Hall and J. Worobec: in *Phase Transformations during the Thermal/Mechanical Processing of Steel*, E.B. Hawbolt and S. Yue, eds., The Metallurgical Society of CIM, Montreal, pp. 305-16.
34. W.P. Sun, E.B. Hawbolt, T.R. Meadowcroft, and J.J. Jonas: *HSLA Steels '95*, G. Liu, H. Stuart, H. Zhang, and C. Li, eds., China Science and Technology Press, Beijing, 1995, pp. 169-74.
35. R. Pandi, M. Militzer, E.B. Hawbolt, and T.R. Meadowcroft: in *Phase Transformations during the Thermal/Mechanical Processing of Steel*, E.B. Hawbolt and S. Yue, eds., The Metallurgical Society of CIM, Montreal, 1995, pp. 459-71.

36. A. Giumelli, M. Militzer, and E.B. Hawbolt: *Iron Steel Inst. Jpn. Int.*, 1999, vol. 39, pp. 271-80.
37. M. Militzer and E.B. Hawbolt: *Grain Growth in Polycrystalline Materials III*, H. Weiland, B.L. Adams, and A.D. Rollett, eds., TMS, Warrendale, PA, 1998, pp. 639-44.
38. M. Militzer, D.Q. Jin, and I.V. Samarasekera: in *Advances in Industrial Materials*, D.S. Wilkinson, W.J. Poole, and A. Alpas, eds., The Metallurgical Society of CIM, Montreal, pp. 63-77.
39. W.P. Sun, M. Militzer, R. Pandi, and E.B. Hawbolt: in *Accelerated Cooling/Direct Quenching of Steels*, R. Asfahani, ed., ASM, Materials Park, OH, 1997, pp. 109-16.
40. W.P. Sun, M. Militzer, E.B. Hawbolt, and T.R. Meadowcroft: *Thermec '97*, T. Chandra and T. Sakai, eds., TMS, Warrendale, PA, 1997, pp. 685-91.
41. W.P. Sun, M. Militzer, E.B. Hawbolt, and T.R. Meadowcroft: *Trans. Iron Steel Soc.*, 1998, vol. 25 (5), pp. 85-94.
42. R. Gjengedal, J.K. Solberg, and X.D. Liu: *HSLA Steels '95*, G. Liu, H. Stuart, H. Zhang, and C. Li, eds., China Science and Technology Press, Beijing, 1995, pp. 357-62.
43. M. Militzer, R. Pandi, E.B. Hawbolt, and T.R. Meadowcroft: in *Accelerated Cooling/Direct Quenching of Steels*, R. Asfahani, ed., ASM, Materials Park, OH, 1997, pp. 151-57.
44. J. Agren: *Scripta Metall.*, 1986, vol. 20, pp. 1507-10.
45. S.V. Subramanian, X. Zheng, L.E. Collins, M. Bucholtz, and M. Kostic: in *Low Carbon Steels for the 90's*, R. Asfahani and G. Tither, eds., TMS, Warrendale, PA, 1993, pp. 313-22.
46. I. Tamura, H. Sekine, T. Tanaka, and C. Ouchi: *Thermomechanical Processing of High Strength Low Alloy Steels*, Butterworth and Co., London, 1988, p. 21.
47. P.C. Campbell, E.B. Hawbolt, and J.K. Brimacombe: *Metall. Trans. A*, 1991, vol. 22A, pp. 2779-90.
48. M. Umemoto, A. Hiramatsu, A. Moriya, T. Watanabe, S. Nanba, N. Nakajima, G. Anan, and Y. Higo: *Iron Steel Inst. Jpn. Int.*, 1992, vol. 32, pp. 306-15.
49. M. Suehiro, K. Sato, Y. Tsukano, H. Yada, T. Senuma, and Y. Matsumura: *Trans. Iron Steel Inst. Jpn.*, 1987, vol. 27, pp. 439-45.
50. R. Priestner and P.D. Hodgson: *Mater. Sci. Technol.*, 1992, vol. 8, pp. 849-54.
51. E.V. Pereloma and J.D. Boyd: *Mater. Sci. Technol.*, 1996, vol. 12, pp. 808-17.
52. M. Militzer, W.P. Sun, W.J. Poole, and P. Purtscher: *Thermec '97*, T. Chandra and T. Sakai, eds., TMS, Warrendale, PA, 1997, pp. 2093-99.
53. L.E. Collins, D.L. Baragar, J.T. Bowker, M.M. Kostic, and S.V. Subramanian: *Microalloying '95*, ISS, Warrendale, PA, 1995, pp. 141-47.
54. G.A. Duit, A. Hurkmans, J.J.F. Scheffer, and T.M. Hoogendoorn: *Thermec '88*, I. Tamura, ed., ISIJ, Tokyo, 1988, pp. 114-21.
55. M. Militzer, W.J. Poole, and W.P. Sun: *Steel Res.*, 1998, vol. 69, pp. 279-85.
56. I.M. Lifshitz and V.V. Slyozov: *J. Phys. Chem. Solids*, 1961, vol. 19, pp. 35-50.
57. C. Wagner: *Z. Electrochem.*, 1961, vol. 65, pp. 581-91.
58. H.R. Shercliff and M.F. Ashby: *Acta Metall. Mater.*, 1990, vol. 38, pp. 1789-1802.
59. L.G.E. Vollrath, R. Hackl, K.G. Schmitt-Thomas, and D. Daub: *Microalloying '88*, ASM, Metals Park, OH, 1988, pp. 353-58.
60. P. Repas: *HSLA Steels: Technology and Applications*, ASM, Metals Park, OH, 1984, pp. 203-08.
61. I.V. Samarasekera, D.Q. Jin, and J.K. Brimacombe: *38th Mechanical Working and Steel Processing Conf. Proc.*, ISS, Warrendale, PA, 1996, vol. XXXIV, pp. 313-27.
62. I.V. Samarasekera, D.Q. Jin, and J.K. Brimacombe: *Thermec '97*, T. Chandra and T. Sakai, eds., TMS, Warrendale, PA, 1997, pp. 57-66.
63. L.E. Collins: in *Materials for Resource Recovery and Transport*, L.E. Collins, ed., The Metallurgical Society of CIM, Montreal, 1998, pp. 251-65.
64. I.V. Samarasekera, C.A. Muojekwu, D.Q. Jin, and J.K. Brimacombe: *39th Mechanical Working and Steel Processing Conf. Proc.*, ISS, Warrendale, PA, 1998, vol. XXXV, pp. 861-73.